Title: Lysophosphatidylcholine acyltransferase 1 suppresses nanoclustering and function of KRAS

Authors: Neha Arora[1], Hong Liang[1], Wantong Yao[3], Haoqiang Ying[4], Junchen Liu[1] and Yong Zhou[1,2,*]

Affiliations: 1. Department of Integrative Biology and Pharmacology, McGovern Medical School, University of Texas Health Science Center, Houston, Texas, USA

2. Program of Biochemistry and Cell Biology, Graduate School of Biological Sciences, M. D. Anderson Cancer Center and University of Texas Health Science Center, Houston, Texas, USA

3. Department of Translational Molecular Pathology, Division of Pathology-Lab Medicine Div, The University of Texas MD Anderson Cancer Center, Houston, Texas, USA

4. Department of Molecular and Cellular Oncology, Division of Basic Science Research, The University of Texas MD Anderson Cancer Center, Houston, Texas, USA

Corresponding author: * Yong Zhou, yong.zhou@uth.tmc.edu

Key Word: KRAS, nanoclustering, Lysophosphatidylcholine acyltransferase 1, phosphatidylserine, acyl chains, electron microscopy, cancer.

Abstract

KRAS is frequently mutated in cancer, contributing to 20% of all human cancer especially pancreatic, colorectal and lung cancer. Signaling of the constitutively active KRAS oncogenic mutants is mostly compartmentalized to proteolipid nanoclusters on the plasma membrane (PM). Signaling nanoclusters of many KRAS mutants selectively enrich phosphatidylserine (PS) lipids with unsaturated *sn-2* acyl chains, but not the fully saturated PS species. Thus, remodeling PS acyl chains may suppress KRAS oncogenesis. Lysophosphatidylcholine acyltransferases (LPCATs) remodel *sn-2* acyl chains of phospholipids, with LPCAT1 preferentially generating the fully saturated lipids. Here, we show that stable expression of LPCAT1 depletes major PS species with unsaturated sn-2 chains while decreasing minor phosphatidylcholine (PC) species with the corresponding acyl chains. LPCAT1 expression more effectively disrupts the nanoclustering of oncogenic GFP-KRAS^{G12V}, which is restored by acute addback of exogenous unsaturated PS. LPCAT1 expression compromises signaling and oncogenic activities of the KRAS-dependent pancreatic tumor lines. LPCAT1 expression sensitizes human pancreatic tumor MiaPaCa-2 cells to KRAS^{G12C} specific inhibitor, Sotorasib. Statistical analyses of patient data further reveal that pancreatic cancer patients with KRAS mutations express less LPCAT1. Higher LPCAT1 expression also improves survival probability of pancreatic and lung adenocarcinoma patients with KRAS mutations. Thus, PS acyl chain remodeling selectively suppresses KRAS oncogenesis.

Introduction

KRAS small GTPase is a molecular switch that toggles between the inactive GDP-bound and active GTP-bound states [1-4]. KRAS activates a wide variety of signaling cascades, including mitogen-activated protein kinases (MAPKs) and phosphoinositol 3 kinase (PI3K), and regulates cell survival, growth, division, proliferation and migration [1-4]. KRAS is one of the most frequently mutated genes in cancer, especially contributing to 98% of pancreatic, 45% of colorectal and 31% of lung tumors [1-4]. Mutations at residues, such as G12, G13 and Q61, of KRAS are prevalent in cancer [1-4]. Traditional strategies of targeting the enzymatic G-domain of KRAS have met significant challenges because its dynamic G-domain lacks stable grooves for small molecules to bind with high affinity. Tumors also quickly develop resistance against inhibition of specific KRAS mutants, in part by generating secondary mutations of KRAS [5-7]. Alternatively, disrupting the spatial distribution of KRAS can suppress signaling and function of KRAS mutants. This is because signaling of wild-type and the constitutively active mutants of KRAS is mostly restricted to proteolipid nanoclusters on the plasma membrane (PM) [1,2,8]. While membrane associations have in general been perceived as lacking specificity, KRAS/membrane association is shown to possess intricate selectivity. It was first reported that KRAS prefers to localize to more fluid and cholesterol-poor liquid-disordered (L_d) or non-raft regions (enriched with unsaturated lipids) of the PM [9-11]. Forcing KRAS into the cholesterol-enriched lipid rafts enriched with saturated lipids abolishes KRAS/MAPK signaling [12-14]. It was then reported that KRAS signaling nanoclusters selectively enrich an anionic phospholipid, phosphatidylserine (PS), more specifically PS species with unsaturated *sn-2* acyl chains [15-24]. Depletion of endogenous PS disrupts the nanoclustering, signaling and oncogenic activities of KRAS mutants [15-20,25-30]. Acute addback of PS species with unsaturated sn-2 acyl chains, but not the fully saturated PS, effectively restores the nanoclustering and effector recruitment of mutant KRAS in the PS-depleted cells [17-21]. Thus, KRAS possesses sensitivity for lipid headgroups (PS) and acyl chains (unsaturated acyl chains).

Mammalian cells typically contain 30-40 PS species, with unsaturated PS species as main components. While direct regulation of PS acyl chain biogenesis is poorly understood, PS is converted from phosphatidylcholine (PC) and phosphatidylethanolamine (PE) through headgroup exchange [31]. Lysophosphatidylcholine acyltransferases (LPCATs) remodel *sn-2* acyl chains of PC and PE with high specificity [32,33]. It is, thus, possible that LPCATs can indirectly remodel PS acyl chains and in turn impact the spatial distribution and oncogenic activities of KRAS. Particularly, LPCAT1 preferentially catalyzes the attachment of fully saturated acyl chains to the *sn-2* position of PC and PE [32,33]. Higher expression of LPCAT1 increases levels of saturated PC and stabilizes the liquid-ordered (L_o) domains [33]. We, here, show that stable expression of LPCAT1 depletes major PS species with unsaturated sn-2 chains and disrupts the nanoclustering and oncogenic activities of KRAS in pancreatic tumor lines. Thus, remodeling PS acyl chains can be a novel strategy to target KRAS oncogenesis.

Results

LPCAT1 expression depletes unsaturated PS in pancreatic tumor cells.

We generated human pancreatic ductal adenocarcinoma (PDAC) MiaPaCa-2 cells stably expressing either empty vector V2 or LPCAT1. Higher LPCAT1 expression in MiaPaCa-2 cells stably expressing LPCAT1 was validated in Western blotting (Inset of Fig.1). Whole-cell lysates of MiaPaCa-2 cells stably expressing V2 or LPCAT1 were collected for shot-gun lipidomics. Changes in acyl chain structures, such as acyl chain length (Supplemental Figure 1) and numbers of double bonds (Supplemental Figure 2), of main lipid types are shown. Main lipid types include phosphatidylcholine (PC), phosphatidic acid (PA), phosphatidylethanolamine (PE), phosphatidylserine (PS), phosphoinositides (PI), sphingomyelin (SM), as well as lysophospholipid species (lyso PC, lyso PE and lyso PA). Detailed changes in species of these lipid types are also shown in Supplemental Figures 3-11. Since KRAS nanoclusters selectively enrich unsaturated

PS species [15-24], we focused on effects of LPCAT1 on PS acyl chain homeostasis. In Fig.1A, when compared with V2 control, MiaPaCa-2 cells expressing LPCAT1 contained significantly lower levels of PS species with unsaturated *sn-2* chains, including 18:0/18:1 PS (comprising 28% of the total PS), 18:0/18:2 PS (9% of the total PS) and 18:0/20:3 PS (28% of the total PS). LPCAT1 expression also elevated levels of 16:0/16:1 PS (0.7% of the total PS) and 16:1/20:1 PS (0.7% of the total PS). Together, LPCAT1 expression decreased 3 major PS species (~65% of the total PS) with mono- or polyunsaturated *sn-2* chains, while increasing minor PS species (~1.4% of the total PS). Consistent with the notion that PS is in part converted from PC species, PC species with the same acyl chains, such as 18:0/18:1 PC, 18:0/18:2 PC and 18:0/20:3 PC, were also depleted in MiaPaCa-2 cells stably expressing LPCAT1 when compared with the V2 control. Interestingly, these PC species combine to account for ~5% of the total PC content. Thus, stable LPCAT1 expression more effectively depletes PS species with unsaturated *sn-2* chains.

LPCAT1 expression disrupts the PM localization and nanoclustering of KRAS^{G12V}.

We next used electron microscopy (EM)- univariate nanoclustering analysis to examine effects of LPCAT1 on signaling nanoclusters of a major oncogenic mutant KRAS^{G12V} ectopically expressed in MiaPaCa-2 cells. MiaPaCa-2 cells stably expressing V2 or LPCAT1 were lentiviral-infected with GFP-KRAS^{G12V}. Basolateral PM sheets of these cells were attached to EM grids. GFP-KRAS^{G12V} anchored to the PM inner leaflet was immunolabeled with anti-GFP antibody conjugated to 4.5 nm gold nanoparticles. The gold-labeled GFP-KRAS^{G12V} was imaged via transmission EM (TEM) at 100,000X magnification. Spatial distribution of gold particles within a 1 μm^2 PM area was quantified using the Ripley's K-function analysis, where the extent of nanoclustering, $L(r) - r$, was plotted against distance r in nanometers. The peak $L(r) - r$ value, or L_{max}, was used as a statistical summary for nanoclustering. $L(r) - r$ values above the 99% confidence interval (99% CI) of 1 indicate statistically significant nanoclustering, with larger L_{max} values corresponding to more

extensive nanoclustering. In Fig.2A, L_{max} of GFP-KRAS^{G12V} in MiaPaCa-2 cells expressing LPCAT1 was significantly decreased (below 99% CI marked by the green line) when compared with L_{max} of GFP-KRAS^{G12V} in MiaPaCa-2 cells expressing V2. This data indicates that LPCAT1 expression effectively abolishes the nanoclustering of GFP-KRAS^{G12V} on the PM. Fig.2B shows that gold labeling of GFP-KRAS^{G12V} per 1 μm^2 of PM area in cells expressing LPCAT1 was also significantly lower than that in the V2-expressing cells, suggesting that LPCAT1 expression significantly mislocalizes GFP-KRAS^{G12V} from the PM. Another RAS isoform, HRAS, distributes to spatially separate nanoclusters enriched with different lipids than KRAS [9,10,15,16,19,20]. LPCAT1 expression partially decreased the nanoclustering of GFP-HRAS^{G12V} (Fig.2C), while having no effect on the PM localization of GFP-HRAS^{G12V} (Fig.2D). Thus, LPCAT expression more effectively disrupts the PM association of a KRAS mutant.

To validate the PS acyl chain specificity, we performed acute addback experiments in baby hamster kidney (BHK) cells stably expressing empty vector pC1 or LPCAT1. Similar to MiaPaCa-2 cells, LPCAT1 expression effectively abolished the nanoclustering of GFP-KRAS^{G12V} (Fig.2E) and mislocalized GFP-KRAS^{G12V} from the PM of BHK cells (Fig.2F). In an acute addback experiment, BHK cells stably expressing LPCAT1 were incubated with medium containing 10 μM exogenous 18:0/18:1 PS for 1 hour before EM-nanoclustering analysis. We chose 18:0/18:1 PS because LPCAT1 expression significantly decreased 18:0/18:1 PS (a major PS species comprising 28% of the total PS, Fig.1A). Acute addback of 18:0/18:1 PS effectively restored the nanoclustering and PM localization of GFP-KRAS^{G12V} (Fig.2E and F). LPCAT1 expression partially and numerically decreased the nanoclustering of GFP-HRAS^{G12V} (Fig.2G) and elevated the PM localization of GFP-HRAS^{G12V} (Fig.2H) in BHK cells, also similar to effects of LPCAT1 on GFP-HRAS^{G12V} in MiaPaCa-2 cells. Acute addback of 18:0/18:1 PS had no effect on the PM localization (Fig.2G) and nanoclustering of GFP-HRAS^{G12V} (Fig.2H). Taken together, LPCAT1

expression more effectively perturbs the PM association of $KRAS^{G12V}$, which is mediated by PS species with unsaturated *sn-2* chains.

LPCAT1 expression suppresses MAPK signaling and oncogenic activities of KRAS-dependent tumor cells.

We next compared effects of LPCAT1 expression on signal output of MAPK and PI3K cascades in the KRAS-dependent human pancreatic tumor lines, including MOH and PANC1 cells, and the KRAS-independent human pancreatic tumor BxPC3 cells. Stable LPCAT1 expression significantly decreased levels of phosphorylated ERK (pERK/total ERK) in MOH and PANC1 cells, while having minimal effect on MAPK signaling in BxPC3 cells (Fig.3A-D). The PI3K signaling (pAkt/total Akt) less preferentially regulated by KRAS was unaffected by LPCAT1 expression (Fig.3A, F-G). Taken together, LPCAT1 expression more effectively decreases MAPK signaling in the KRAS-dependent tumor lines.

We then compared effects of LPCAT1 on oncogenic activities of MOH and BxPC3 cells. MOH stably expressing LPCAT1 displayed fewer number of colonies than MOH cells expressing V2 control, while having no effect on colony formation of BxPC3 cells (Fig.4A-C). LPCAT1 expression also significantly decreased proliferation of MOH cells, while having no effect on BxPC3 cells (Fig.4D and E). To further evaluate the specificity of LPCAT1, we used iKRAS line, a murine PDAC line with doxycycline (DOX)-induced expression of $KRAS^{G12D}$ [7,34]. Stable expression of LPCAT1 significantly decreased colony sizes of iKRAS cells with the induced expression of $KRAS^{G12D}$ (DOX+), while having no effect on colony sizes of iKRAS cells without KRAS mutant (DOX-) (Fig.4F). Taken together, LPCAT1 more preferentially suppresses oncogenic activities of KRAS-driven tumor cells.

To evaluate effects of LPCAT1 on cancer cell migration, we performed a scratch assay using MiaPaCa-2 cells, a metastasis model. MiaPaCa-2 cells stably expressing V2 or LPCAT1 were seed to confluency. Twenty-four hours following a scratch, gaps between cells were measured to indicate wound healing capacity and migration. In Fig.5, gap of MiaPaCa-2 cells expressing LPCAT1 was significantly wider than MiaPaCa-2 cells expressing V2. Thus, LPCAT1 expression results in slower migration of MiaPaCa-2 cells.

LPCAT1 chemosensitizes KRAS specific inhibitor.

To examine effects of LPCAT1 on chemosensitization of KRAS-dependent tumor cells, we treated MiaPaCa-2 cells stably expressing V2 or LPCAT1 with $KRAS^{G12C}$-specific inhibitor Sotorasib. In Fig.6A, Sotorasib further decreased proliferation of MiaPaCa-2 cells stably expressing LPCAT1 when compared with MiaPaCa-2 cells expressing V2. We next treated MiaPaCa-2 cells with Trametinib, a MEK inhibitor. In Fig.6B, LPCAT1 expression did not impact the inhibitory effects of Trametinib on proliferation of MiaPaCa-2 cells. Our data suggest that KRAS activities are sensitive to LPCAT1 expression.

LPCAT1 expression correlates with KRAS oncogenesis in patients.

To further examine correlation between LPCAT1 and KRAS oncogenesis in patients, we performed statistical analysis using patient data obtained from the Cancer Genomic Atlas (TCGA) in the Genomic Data Commons (GDC) data portal. We show that pancreatic cancer patients with KRAS-dependent tumors contained significantly lower LPCAT1 expression than those with KRAS-independent tumors (Fig.7A). Kaplan Meier analysis illustrated that pancreatic cancer patients with higher LPCAT1 expression possessed higher survival probability than those with lower LPCAT1 expression (Fig.7B). Further Kaplan Meier analysis revealed that higher LPCAT1

expression significantly improved the survival probability of patients with KRAS-dependent lung cancer (Fig.7C). On the other hand, lung cancer patients with KRAS-independent tumors did not display any correlation between LPCAT1 expression and survival probability (Fig.7D). Taken together, higher LPCAT1 expression improves prognosis of patients with KRAS-dependent tumors.

Discussion

Because of its high prevalence in cancer, KRAS has been a major focus in drug discovery efforts. Recently, the FDA approved the use of Sotorasib and Adagrasib in treatment of non-small cell lung cancer [35,36]. Both Sotorasib and Adagrasib specifically target $KRAS^{G12C}$ and covalently modify the cysteine mutation at the G12 position [35,36]. Alternatively, the spatial distribution of KRAS mutants can be perturbed to compromise their oncogenic activities since it has long been observed that KRAS signaling is mostly restricted to the PM [2,8,37]. An essential step in facilitating the PM anchoring of KRAS involves prenylation of its C-terminal CAAX motif [16-18,38]. However, earlier attempts to inhibit the prenylation of KRAS via farnesyltransferase inhibitors (FTIs) have not been successful since KRAS mutants are alternatively geranylgeranylated in the presence of FTIs [39-41]. This experience has considerably dampened the enthusiasm of targeting the membrane association of KRAS. Later studies using quantitative imaging, biophysical assays and molecular dynamic simulations revealed intricate selectivity in the PM anchoring of KRAS [15-30]. To efficiently recruit effectors and propagate signaling, KRAS must incorporate into nanoclusters with precise lipid contents, especially PS lipids with unsaturated *sn-2* acyl chains, on the PM [15-30]. Cells use tightly regulated networks of lipid metabolism pathways to maintain precise homeostasis of lipids with a wide variety of acyl chain structures. Our current study explored how remodeling PS acyl chains in cancer cells may impact KRAS signaling and activities. We show that higher expression of LPCAT1 depletes major PS species with unsaturated *sn-2* chains, more effectively suppresses

the PM nanoclustering, signaling and oncogenic activities of KRAS mutants. Pancreatic cancer patients with KRAS mutations express lower LPCAT1 levels. Higher LPCAT1 levels in pancreatic and lung cancer patients expressing KRAS mutants significantly improve the prognosis. Further, human pancreatic tumor cells expressing higher LPCAT1 levels are more sensitive to KRAS inhibitors. Thus, LPCAT1 may be a new target when considering treatment options for KRAS cancer.

LPCAT1 expression has been shown to promote oncogenic activities of epidermal growth factor receptor (EGFR)-driven cancer by elevating levels of the fully saturated PC and promoting lipid rafts [33]. We now show that increasing expression of LPCAT1 inhibits oncogenic activities of KRAS mutants in pancreatic tumor cells, and negatively correlates with KRAS oncogenesis in pancreatic and lung cancer patients. This reflects complex biological and pathological roles of LPCAT1 and intricate selectivity of lipid acyl chain remodeling. EGFR dimerization/oligomerization occur in the L_o domains or lipid rafts enriched with cholesterol and saturated lipids, which in turn promotes autophosphorylation and signaling [33,42]. On the other hand, KRAS activities occur away from cholesterol in cells [9,10,12,15,17-20]. We recently showed that the PM nanoclusters of KRAS oncogenic mutants, such as $KRAS^{G12C}$, $KRAS^{G12D}$, $KRAS^{G12V}$, $KRAS^{G13D}$ and $KRAS^{Q61H}$, contain PS species with the unsaturated *sn-2* chains [20]. Surface plasmon resonance (SPR) further revealed that the purified KRAS more efficiently binds to model bilayers comprising the unsaturated PS species, but not the saturated PS species [21]. Atomic force microscopy (AFM) and molecular dynamic (MD) simulations showed that KRAS molecules prefer to distribute to the cholesterol-poor L_d domains enriched with unsaturated lipids [11,43,44]. Nanoclustering of wild-type KRAS and $KRAS^{G12V}$ on the cell PM is independent of cholesterol depletion [9,18]. Trapping KRAS to lipid rafts abolishes effector binding and the KRAS-dependent MAPK signaling [12-14]. Presence of saturated lipids in the nanoclusters of KRAS mutants also compromises recruitment of effector CRAF [17,20]. Thus, the opposing effects of LPCAT1 on EGFR

and KRAS are consistent with the opposing lipid preferences of these two membrane proteins. Taken together, remodeling lipid acyl chains impacts cell signaling events on membranes in distinct manners.

Since membranes provide platforms for many proteins, perturbing lipid metabolism and membrane properties has been assumed to lack specificity. Interestingly, we observed that LPCAT1 more preferentially targets oncogenic activities of the KRAS-dependent pancreatic tumor cells, while having little effects on the KRAS-independent cells, suggesting that lipid-dependent signaling is more selective than previously thought. A possible explanation is that PC species affected by higher LPCAT1 expression are mostly minor PC species. For example, LPCAT1 expression decreases PC and PS species with the same acyl chains, such as 18:0/18:1, 18:0/18:2 and 18:0/20:3 (Fig.1). While PS species with these acyl chains are major PS species (together comprising ~65% of total PS), the PC counterparts are minor PC species (together accounting for 5.6% of total PC). Thus, the PS-dependent signaling platforms, such as KRAS nanoclusters, are more sensitive to LPCAT1 expression. Further, tumor cells transformed by KRAS mutants become addicted to the prevalent KRAS signaling, whereas the wild-type KRAS-expressing cells rely on a plethora of balanced signaling cascades or are addicted to other oncogenic signaling events for essential activities. This causes the KRAS-transformed tumor cells to be more sensitive to perturbations of PS homeostasis.

Conclusion

PS species with unsaturated *sn-2* chains are enriched in the signaling nanoclusters of KRAS oncogenic mutants. Altering homeostasis of PS species may be an alternative strategy to inhibit KRAS oncogenesis. Here, we show that higher LPCAT1 expression depletes major unsaturated PS species and perturb the nanoclustering and signaling of KRAS oncogenic mutants. Concordantly, higher LPCAT1 expression improves the prognosis of pancreatic and lung cancer

patients with KRAS-dependent tumors. Thus, LPCAT1 may serve as a marker when considering treatment options for the KRAS-dependent cancer. In the future, specific promoters of LPCAT1, or inhibitors of LPCAT1 antagonists, may be explored as alternative treatment strategies for KRAS cancer.

Acknowledgements

This work was supported in part by the National Institutes of Health R01GM138668 to N. Arora, H. Liang and Y. Zhou.

Materials and Methods

Electron microscopy (EM)-spatial analysis

EM-univariate nanoclustering

Apical or basolateral PM of baby hamster kidney (BHK) or human pancreatic tumor MiaPaCa-2 cells expressing GFP-KRAS^{G12V} or GFP-HRAS^{G12V} was attached to EM grids. The intact native PM sheets were then fixed with 4% paraformaldehyde (PFA) / 0.1% gluaraldehyde, tagged with anti-GFP antibody conjugated with 4.5 nm gold nanoparticles, and negative stained with 0.3% uranyl acetate, and embedded in methyl cellulose. Transmission EM (TEM) was used to image PM sheets at 100,000x magnification. ImageJ was then used to assign the x / y coordinates of each gold particle within a select 1μm^2 PM area. Ripley's K-function calculated the nanoclustering of the gold-labeled GFP-RAS on the PM. The null hypothesis of this analysis is that the gold nanoparticles distribute in a random pattern:

$$K(r) = \mathrm{A}n^{-2} \sum_{i \neq j} w_{ij} 1(\|x_i - x_j\| \leq r) \qquad \text{(Eq. A)}$$

$$L(r) - r = \sqrt{\frac{K(r)}{\pi}} - r \qquad \text{(Eq. B)}$$

In Equation A, $K(r)$ denotes the univariate distribution for gold nanoparticles with a total number of n in a PM area of A; r signifies the distance between gold particles with an increment of 1 nm from 1 to 240 nm; $\|\cdot\|$ denotes Euclidean distance that describes an indicator of $1(\cdot) = 1$ if $\|x_i - x_j\| \leq r$ and $1(\cdot) = 0$ if $\|x_i - x_j\| > r$. w_{ij}^{-1} is used to correct edge effects by describing the fraction of the circumference of a circle with the center defined as x_i and radius $\|x_i - x_j\|$. In Equation B, $L(r) - r$ denotes the linear transformation of $K(r)$ in Eq. A, which is achieved by normalizing $K(r)$ against the 99% confidence interval (99% C.I.) calculated via Monte Carlo simulations. $L(r) - r = 0$ when gold nanoparticles distribute a complete random pattern. $L(r) - r$ values above the 99% confidence interval (99% CI) of 1 indicate statistically meaningful clustering, with larger $L(r) - r$ values describing more extensive clustering. The peak values of $L(r) - r$ curves, termed as L_{max}, are used as a summary statistic to signify the extent of nanoclustering. For each condition, at least 15 PM sheets from individual cells were imaged, analyzed and pooled. Statistical significance was evaluated via comparing our calculated point patterns against 1000 bootstrap samples in bootstrap tests [16,17].

EM-Bivariate co-clustering analysis

The K-function bivariate co-clustering analysis quantifies the co-clustering between two differently sized gold nanoparticles tagging two different constituents on the intact PM sheets [16,17]. Similar to the univariate nanoclustering protocol described above, intact apical PM sheets of PSA3 cells co-expressing GFP-LactC2 (probing PS lipids) and an RFP-tagged RAS construct were attached to EM grids and fixed with 4% PFA and 0.1% gluaraldehyde. The PM sheets were incubated with 6 nm gold nanoparticles linked to anti-GFP antibody, blocked with 0.2% bovine serum albumin (BSA) and 0.2% fish skin gelatin, then incubated with 2 nm gold conjugated to anti-RFP antibody. ImageJ was used to assign coordinates to the gold nanoparticle. A bivariate K-function analysis

tested the null hypothesis that the two populations of gold particles spatially separate from each other. (Eqs. C-F):

$$K_{biv}(r) = (n_b + n_s)^{-1}[n_b K_{sb}(r) + n_s K_{bs}(r)] \quad \text{(Eq. C)}$$

$$K_{bs}(r) = \frac{A}{n_b n_s} \sum_{i=1}^{n_b} \sum_{j=1}^{n_s} w_{ij} 1(\|x_i - x_j\| \leq r) \quad \text{(Eq. D)}$$

$$K_{sb}(r) = \frac{A}{n_b n_s} \sum_{i=1}^{n_s} \sum_{j=1}^{n_b} w_{ij} 1(\|x_i - x_j\| \leq r) \quad \text{(Eq. E)}$$

$$L_{biv}(r) - r = \sqrt{\frac{K_{biv}(r)}{\pi}} - r \quad \text{(Eq. F)}$$

where $K_{biv}(r)$ denotes a bivariate estimator and contains two individual bivariate K-functions: $K_{bs}(r)$ quantifies how the big 6 nm gold particles (*b* = big gold) distribute around each 2 nm small gold particle (*s* = small gold); $K_{sb}(r)$ describes how small gold particles distribute around each big gold particle. The value of n_b indicates the number of 6 nm big gold and n_s indicates the number of 2nm small gold within a PM area of *A*. Other parameters denote the same definitions as defined in the univariate calculations in Eqs.A and B. $L_{biv}(r)$-*r* is a linearly transformation of $K_{biv}(r)$, and is normalized against the 95% confidence interval (95% C.I.). An $L_{biv}(r)$-*r* value of 0 indicates spatial segregation between the two populations of gold particles, whereas an $L_{biv}(r)$-*r* value above the 95% C.I. of 1 at the corresponding distance of *r* indicates yields statistically significant co-localization at certain distance yields. Area-under-the-curve for each $L_{biv}(r)$-*r* curves was calculated within a fixed range $10 < r < 110$ nm, and was termed bivariate $L_{biv}(r)$-*r* integrated (or LBI):

$$LBI = \int_{10}^{110} Std\ L_{biv}(r) - r\,.dr \quad \text{(Eq. G)}$$

For each condition, > 15 apical PM sheets were imaged, analyzed and pooled, shown as mean of LBI values ± SEM. Statistical significance between conditions was evaluated via comparing against 1000 bootstrap samples as described [16,17].

Cell culturing and generation of stable lines

Human and murine pancreatic tumor cell lines, including MOH, PANC1, BxPC3 and iKRAS cells, were maintained in DMEM medium containing 10% fetal bovine serum (FBS). PDAC cell line MiaPaCa-2 was maintained in DMEM medium containing 10% fetal bovine serum (FBS) and 2.5% horse serum (HS). To generate stable cell lines, the pEF6 vector plasmid without/with the cDNA of human LPCAT1 was used to transfect the tumor cells. For each line, 1 μg of plasmid was added to 7 μl of lipofectamine for the transfection. Following 5-hour incubation with the plasmids, cells were washed and changed to DMEM medium containing 10% FBS and 3 μg/mL puromycin antibiotic. Cells were grown in the presence of antibiotics for a week before serial dilution and seeding in 96-well plates with a concentration of < 1 cell per well. Cell colonies were then harvested for Western blotting to verify the expression of LPCAT1.

Western blotting

Whole-cell lysates of MOH, PANC1 and BxPC3 cells were collected. Following electrophoresis in SDS PAGE gels and transfer, membranes were incubated with primary antibodies against the phosphorylated ERK and Akt, total ERK and Akt, LPCAT1, as well as loading control of actin, overnight. After secondary antibody incubation, membranes were imaged using enhanced chemiluminescence (ECL) solution. Data are shown as mean ± SEM. ImageJ software analysis was used to evaluate expression intensity and identify fold change.

Proliferation

CyQUANT cell proliferation assay was used to measure number of live cells in microplates. Appropriate number of PDAC cells, such as MOH (1000 cells/well), MiaPaCa-2 (2000 cells/well) and BxPC3 (3000 cells/well), were seeded in 96-well plates. After 96 hours, cells were washed and stained with CyQUANT® GR dye. Following lysis, fluorescence of dye bound to intact nucleic acids was measured using a Tecan plate reader. For each condition, 3 independent experiments

were performed, and data were pooled together. Student's t-test was used to evaluate the statistical significance.

Colony formation

All human and murine pancreatic cancer cell lines stably expressing V2 or LPCAT1 were seeded in 6-well plates. Specifically, iKRAS (400 cells/well), MOH (250 cells/well) cells were grown for 7 days. MiaPaCa-2 (100 cells/well) were grown for 10 days and BxPC3 (1000 cells/well) were grown for 14 days. Cells were washed twice with PBS, followed with fixation with 4% paraformaldehyde for 15 min. Cell staining was performed with 0.01% crystal violet for 15 min. Colony images were captured using Perkin Elmer X3 multiplate reader. Colony count was performed using ImageJ. For each condition, 3 independent experiments were conducted. Student's t-test was used to evaluate the statistical significance.

Wound healing scratch assay

We performed wound healing assay to compare migration of MiaPaCa-2 cells. MiaPaCa-2 cells were seeded in 35mm cell culture dishes and allowed to grow to confluency. The plates were scratched to create a gap in the monolayer of cells. The plates were imaged at different time points within 24 hours using EVOS M5000 microscope imaging system and width of the gap was measured using ImageJ.

Bibliography

1 McCormick, F. Progress in targeting RAS with small molecule drugs. *Biochem J* **476**, 365-374 (2019). https://doi.org:10.1042/BCJ20170441

2 Cox, A. D., Der, C. J. & Philips, M. R. Targeting RAS Membrane Association: Back to the Future for Anti-RAS Drug Discovery? *Clinical cancer research : an official journal of the American Association for Cancer Research* **21**, 1819-1827 (2015). https://doi.org:10.1158/1078-0432.CCR-14-3214

3 Cox, A. D., Fesik, S. W., Kimmelman, A. C., Luo, J. & Der, C. J. Drugging the undruggable RAS: Mission possible? *Nature reviews. Drug discovery* **13**, 828-851 (2014). https://doi.org:10.1038/nrd4389

4 Prior, I. A., Hood, F. E. & Hartley, J. L. The Frequency of Ras Mutations in Cancer. *Cancer Res* **80**, 2969-2974 (2020). https://doi.org:10.1158/0008-5472.CAN-19-3682

5 Awad, M. M. *et al.* Acquired Resistance to KRAS(G12C) Inhibition in Cancer. *N Engl J Med* **384**, 2382-2393 (2021). https://doi.org:10.1056/NEJMoa2105281

6 Feng, S. *et al.* A saturation mutagenesis screen uncovers resistant and sensitizing secondary KRAS mutations to clinical KRAS(G12C) inhibitors. *Proc Natl Acad Sci U S A* **119**, e2120512119 (2022). https://doi.org:10.1073/pnas.2120512119

7 Lv, X. *et al.* Modulation of the proteostasis network promotes tumor resistance to oncogenic KRAS inhibitors. *Science* **381**, eabn4180 (2023). https://doi.org:10.1126/science.abn4180

8 Simanshu, D. K., Philips, M. R. & Hancock, J. F. Consensus on the RAS dimerization hypothesis: Strong evidence for lipid-mediated clustering but not for G-domain-mediated interactions. *Mol Cell* **83**, 1210-1215 (2023). https://doi.org:10.1016/j.molcel.2023.03.008

9 Prior, I. A., Muncke, C., Parton, R. G. & Hancock, J. F. Direct visualization of Ras proteins in spatially distinct cell surface microdomains. *J Cell Biol* **160**, 165-170 (2003).

10 Plowman, S. J., Muncke, C., Parton, R. G. & Hancock, J. F. H-ras, K-ras, and inner plasma membrane raft proteins operate in nanoclusters with differential dependence on the actin cytoskeleton. *Proc Natl Acad Sci U S A* **102**, 15500-15505 (2005). https://doi.org:0504114102 [pii] 10.1073/pnas.0504114102

11 Weise, K. *et al.* Membrane-mediated induction and sorting of K-Ras microdomain signaling platforms. *J Am Chem Soc* **133**, 880-887 (2011). https://doi.org:10.1021/ja107532q

12 Inder, K. *et al.* Activation of the MAPK module from different spatial locations generates distinct system outputs. *Mol Biol Cell* **19**, 4776-4784 (2008). https://doi.org:E08-04-0407 [pii] 10.1091/mbc.E08-04-0407

13 Ariotti, N. *et al.* Caveolae regulate the nanoscale organization of the plasma membrane to remotely control Ras signaling. *J Cell Biol* **204**, 777-792 (2014). https://doi.org:10.1083/jcb.201307055

14 Zhou, Y., Cho, K. J., Plowman, S. J. & Hancock, J. F. Nonsteroidal anti-inflammatory drugs alter the spatiotemporal organization of Ras proteins on the plasma membrane. *J Biol Chem* **287**, 16586-16595 (2012). https://doi.org:M112.348490 [pii] 10.1074/jbc.M112.348490

15 Zhou, Y. *et al.* Signal Integration by Lipid-Mediated Spatial Cross Talk between Ras Nanoclusters. *Mol Cell Biol* **34**, 862-876 (2014). https://doi.org:10.1128/MCB.01227-13 MCB.01227-13 [pii]

16 Zhou, Y. *et al.* SIGNAL TRANSDUCTION. Membrane potential modulates plasma membrane phospholipid dynamics and K-Ras signaling. *Science* **349**, 873-876 (2015). https://doi.org:10.1126/science.aaa5619

17 Zhou, Y. *et al.* Lipid-Sorting Specificity Encoded in K-Ras Membrane Anchor Regulates Signal Output. *Cell* **168**, 239-251 e216 (2017). https://doi.org:10.1016/j.cell.2016.11.059
18 Zhou, Y., Prakash, P. S., Liang, H., Gorfe, A. A. & Hancock, J. F. The KRAS and other prenylated polybasic domain membrane anchors recognize phosphatidylserine acyl chain structure. *Proc Natl Acad Sci U S A* **118** (2021). https://doi.org:10.1073/pnas.2014605118
19 Liang, H. *et al.* Membrane curvature sensing of the lipid-anchored K-Ras small GTPase. *Life Sci Alliance* **2** (2019). https://doi.org:10.26508/lsa.201900343
20 Arora, N., Mu, H., Liang, H., Zhao, W. & Zhou, Y. RAS G-domains allosterically contribute to the recognition of lipid headgroups and acyl chains. *J Cell Biol* **223** (2024). https://doi.org:10.1083/jcb.202307121
21 Lakshman, B. *et al.* Quantitative biophysical analysis defines key components modulating recruitment of the GTPase KRAS to the plasma membrane. *J Biol Chem* **294**, 2193-2207 (2019). https://doi.org:10.1074/jbc.RA118.005669
22 Koester, A. M., Tao, K., Szczepaniak, M., Rames, M. J. & Nan, X. Nanoscopic Spatial Association between Ras and Phosphatidylserine on the Cell Membrane Studied with Multicolor Super Resolution Microscopy. *Biomolecules* **12** (2022). https://doi.org:10.3390/biom12081033
23 Lee, Y. *et al.* High-throughput, single-particle tracking reveals nested membrane domains that dictate KRas(G12D) diffusion and trafficking. *Elife* **8** (2019). https://doi.org:10.7554/eLife.46393
24 Ozdemir, E. S., Koester, A. M. & Nan, X. Ras Multimers on the Membrane: Many Ways for a Heart-to-Heart Conversation. *Genes (Basel)* **13** (2022). https://doi.org:10.3390/genes13020219
25 Cho, K. J. *et al.* Inhibition of Acid Sphingomyelinase Depletes Cellular Phosphatidylserine and Mislocalizes K-Ras from the Plasma Membrane. *Mol Cell Biol* **36**, 363-374 (2015). https://doi.org:10.1128/MCB.00719-15
26 van der Hoeven, D. *et al.* Fendiline inhibits K-Ras plasma membrane localization and blocks K-Ras signal transmission. *Mol Cell Biol* **33**, 237-251 (2013). https://doi.org:10.1128/MCB.00884-12 MCB.00884-12 [pii]
27 van der Hoeven, D. *et al.* Sphingomyelin metabolism is a regulator of KRAS function. *Mol Cell Biol* (2017). https://doi.org:10.1128/MCB.00373-17
28 Kattan, W. E. *et al.* Targeting plasma membrane phosphatidylserine content to inhibit oncogenic KRAS function. *Life Sci Alliance* **2** (2019). https://doi.org:10.26508/lsa.201900431
29 Kattan, W. E. *et al.* Components of the phosphatidylserine endoplasmic reticulum to plasma membrane transport mechanism as targets for KRAS inhibition in pancreatic cancer. *Proc Natl Acad Sci U S A* **118** (2021). https://doi.org:10.1073/pnas.2114126118
30 Liu, J. *et al.* Glycolysis regulates KRAS plasma membrane localization and function through defined glycosphingolipids. *Nat Commun* **14**, 465 (2023). https://doi.org:10.1038/s41467-023-36128-5
31 Lee, S. *et al.* Impaired retrograde membrane traffic through endosomes in a mutant CHO cell defective in phosphatidylserine synthesis. *Genes Cells* **17**, 728-736 (2012). https://doi.org:10.1111/j.1365-2443.2012.01622.x
32 Harayama, T. *et al.* Lysophospholipid acyltransferases mediate phosphatidylcholine diversification to achieve the physical properties required in vivo. *Cell Metab* **20**, 295-305 (2014). https://doi.org:10.1016/j.cmet.2014.05.019
33 Bi, J. *et al.* Oncogene Amplification in Growth Factor Signaling Pathways Renders Cancers Dependent on Membrane Lipid Remodeling. *Cell Metab* **30**, 525-538 e528 (2019). https://doi.org:10.1016/j.cmet.2019.06.014

34 Ying, H. *et al.* Oncogenic Kras maintains pancreatic tumors through regulation of anabolic glucose metabolism. *Cell* **149**, 656-670 (2012). https://doi.org:10.1016/j.cell.2012.01.058
35 Skoulidis, F. *et al.* Sotorasib for Lung Cancers with KRAS p.G12C Mutation. *N Engl J Med* **384**, 2371-2381 (2021). https://doi.org:10.1056/NEJMoa2103695
36 Janne, P. A. *et al.* Adagrasib in Non-Small-Cell Lung Cancer Harboring a KRAS(G12C) Mutation. *N Engl J Med* **387**, 120-131 (2022). https://doi.org:10.1056/NEJMoa2204619
37 Morstein, J. *et al.* Direct Modulators of K-Ras-Membrane Interactions. *ACS Chem Biol* **18**, 2082-2093 (2023). https://doi.org:10.1021/acschembio.3c00413
38 Hancock, J. F., Paterson, H. & Marshall, C. J. A polybasic domain or palmitoylation is required in addition to the CAAX motif to localize p21ras to the plasma membrane. *Cell* **63**, 133-139 (1990). https://doi.org:0092-8674(90)90294-O [pii]
39 Cox, A. D., Hisaka, M. M., Buss, J. E. & Der, C. J. Specific isoprenoid modification is required for function of normal, but not oncogenic, Ras protein. *Mol Cell Biol* **12**, 2606-2615 (1992). https://doi.org:10.1128/mcb.12.6.2606
40 Hancock, J. F., Cadwallader, K. & Marshall, C. J. Methylation and proteolysis are essential for efficient membrane binding of prenylated p21K-ras(B). *EMBO J* **10**, 641-646 (1991).
41 Baines, A. T., Xu, D. & Der, C. J. Inhibition of Ras for cancer treatment: the search continues. *Future Med Chem* **3**, 1787-1808 (2011). https://doi.org:10.4155/fmc.11.121
42 Schultz, D. F., Billadeau, D. D. & Jois, S. D. EGFR trafficking: effect of dimerization, dynamics, and mutation. *Front Oncol* **13**, 1258371 (2023). https://doi.org:10.3389/fonc.2023.1258371
43 Janosi, L., Li, Z., Hancock, J. F. & Gorfe, A. A. Organization, dynamics, and segregation of Ras nanoclusters in membrane domains. *Proc Natl Acad Sci U S A* **109**, 8097-8102 (2012). https://doi.org:10.1073/pnas.1200773109
44 Janosi, L. & Gorfe, A. A. Segregation of negatively charged phospholipids by the polycationic and farnesylated membrane anchor of Kras. *Biophys J* **99**, 3666-3674 (2010). https://doi.org:S0006-3495(10)01319-6 [pii] 10.1016/j.bpj.2010.10.031

Figure Legends

Figure 1. LPCAT1 expression depletes PS species with unsaturated sn-2 chains. MiaPaCa-2 cells stably expressing empty vector V2 or human LPCAT1 were harvested for lipidomics. (A) Western blotting shows significant increase in the level of LPCAT1 expression in MiaPaCa-2 cells stably expressing LPCAT1 than MiaPaCa-2 cells stably expressing V2 control. PS species (B) and PC species (C) with the corresponding acyl chain structures in MiaPaCa-2 cells expressing V2 or LPCAT1 were compared. Insets show the profiles of PS and PC species. The PS and PC species altered by LPCAT1 stable expression were marked in the charts. For each line, 3 independent experiments were performed. Data were pooled together and shown as mean ± SEM. Student's t-test was used to evaluate the statistical significance, with * indicating $p < 0.05$.

Figure 2. LPCAT1 more preferentially disrupts the signaling nanoclusters of KRAS^{G12V} on the plasma membrane. Spatial distribution of mammalian cells, including human pancreatic ductal adenocarcinoma MiaPaCa-2 and baby hamster kidney (BHK) cells, were quantified via electron microscopy (EM)-spatial analysis. Intact PM sheets of MiaPaCa-2 (A-D) and BHK (E-H) cells stably expressing V2 or LPCAT1 transiently expressing GFP-KRAS^{G12V} or GFP-HRASG12V were attached to EM grids. GFP anchored to the PM inner leaflet was immunolabeled with anti-GFP antibody conjugated to 4.5 nm gold nanoparticles. Distribution of the gold-labeled GFP-KRAS^{G12V} and GFP-HRAS^{G12V} within a selected 1μm^2 PM area was calculated using the Ripley's K-function analysis. A nanoclustering curve was plotted as the extent of nanoclustering, $L(r) - r$, vs. length scale, r in nanometers. The peak value of the curve, termed as L_{max}, was used as a summary statistic to indicate nanoclustering (A, C, E and G). The $L(r) - r$ of 1 is the 99% confidence interval (99% CI, green lines), the values above which indicate statistically meaningful clustering. Number of gold particles within the 1μm^2 PM area was counted to indicate PM localization (B, D, F and H). The nanoclustering and PM localization of GFP-KRAS^{G12V} and GFP-

HRAS^{G12V} of MiaPaCa-2 cells (A-D) and BHK cells (E-H), are shown as mean ± SEM. For the nanoclustering data, the statistical significance was evaluated via the non-parametric bootstrap tests. For the gold labeling data, the statistical significance was quantified using the one-way ANOVA. * indicates $p < 0.05$.

Figure 3. LPCAT1 preferentially decreases MAPK signaling in the KRAS-dependent tumor lines. (A) Whole-cell lysates of human pancreatic tumor lines, including the KRAS-dependent MOH / PANC1 and the KRAS-independent BxPC3 cells stably expressing V2 or LPCAT1, were collected for Western blotting. Antibodies against the phosphorylated ERK (pERK), total ERK, pAkt, total Akt and LPCAT1 were used to blot for targeted proteins. Sample blots for a single trial are shown. Quantifications of pERK/total ERK for MOH (B), PANC1 (C) and BxPC3 (D), as well as pAkt/total Akt for MOH (E), PANC1 (F) and BxPC3 (G), are shown as mean ± SEM pooled from 3 independent experiments. Statistical significance was evaluated using Student's t-test, with * indicating $p < 0.05$.

Figure 4. LPCAT1 preferentially compromises oncogenic activities of the KRAS-dependent tumor lines. The KRAS-dependent MOH and KRAS-independent BxPC3 cells stably expressing V2 or LPCAT1 were seeded in 6-well plates. Colonies were counted after 96 hours of growth. The number of colonies for MOH (A) and BxPC3 (B) are shown as mean ± SEM pooled from 3 independent trials. (C) Sample images of MOH and BxPC3 colonies are shown. To evaluate proliferation, MOH (D) and BxPC3 (E) cells stably expressing V2 or LPCAT1 were seeded in 96-well plates. After 96 hours of growth, CyQUANT cell proliferation assay was used to measure proliferation. Data are shown as mean ± SEM pooled from 3 independent experiments. (F) To further validate the KRAS specificity of LPCAT1 expression, we used murine pancreatic

adenocarcinoma iKRAS cells with inducible expression of $KRAS^{G12D}$. iKRAS cells were maintained in doxycycline (DOX+) to induce expression of $KRAS^{G12D}$, or withdrawn from DOX for 48 hours (DOX-) for KRAS independent condition. iKRAS (DOX+/-) cells were seeded in 6-well plates. After 96 hours, sizes of the colonies were measured. Data are shown as mean ± SEM pooled from 3 independent trials. For all experiments, Student's t-test was used to evaluate the statistical significance with * indicating $p < 0.05$.

Figure 5. LPCAT1 compromises migration of pancreatic tumor cells. Human pancreatic adenocarcinoma MiaPaCa-2 cells stably expressing V2 or LPCAT1 were seeded on 6-well plates and allowed to grow to confluency. A gap was created in the cell monolayer and was measured after 24 hours. (A) Sample images of the wound healing process of MiaPaCa-2 cells are shown. (B) Quantification of the width of gaps is shown as mean ± SEM pooled from 3 independent experiments. Student's t-test was used to evaluate the statistical significance, with * indicating $p < 0.05$.

Figure 6. Pancreatic tumor cells with higher LPCAT1 expression are more sensitive to KRAS inhibition. MiaPaCa-2 cells ($KRAS^{G12C}$) stably expressing V2 or LPCAT1 were treated with different doses of a $KRAS^{G12C}$-specific inhibitor Sotorasib (A) or MEK inhibitor Trametinib (B). CyQUANT cell proliferation assay measured the extent of proliferation. Data are shown as mean ± SEM pooled from 3 independent experiments. Student's t-test was used to evaluate the statistical significance, with * indicating $p < 0.05$.

Figure 7. Higher LPCAT1 expression improves prognosis of the KRAS-dependent pancreatic and lung cancer patients. Statistical analyses were performed using patient data

obtained from the Cancer Genomic Atlas (TCGA) in the Genomic Data Commons (GDC) data portal. (A) LPCAT1 mRNA levels were compared in pancreatic cancer patients with the KRAS-dependent and -independent tumors. Welch's t-tests were performed to evaluate the statistical significance. Kaplan Meier analyses were performed to estimate survival probability of pancreatic cancer patients with high or low LPCAT1 levels (B), as well as effects of high or low LPCAT1 expression on survival probability between the KRAS-dependent (C) and the KRAS-independent tumors (D). For Kaplan Meier curve of pancreatic adenocarcinoma, LPCAT1 $\log_2$ mRNA < 17.29 is defined as low LPCAT1, while LPCAT1 $\log_2$ mRNA > 17.98 is defined as high LPCAT1. For Kaplan Meier curve of lung adenocarcinoma patients with mutant KRAS, LPCAT1 $\log_2$ mRNA < 20.29 is defined as low LPCAT1, while LPCAT1 $\log_2$ mRNA > 21.96 is defined as high LPCAT1. For Kaplan Meier curve of lung adenocarcinoma patients with wild-type KRAS, LPCAT1 $\log_2$ mRNA < 20.27 is defined as low LPCAT1, while LPCAT1 $\log_2$ mRNA > 21.79 is defined as high LPCAT1.

Figure 1

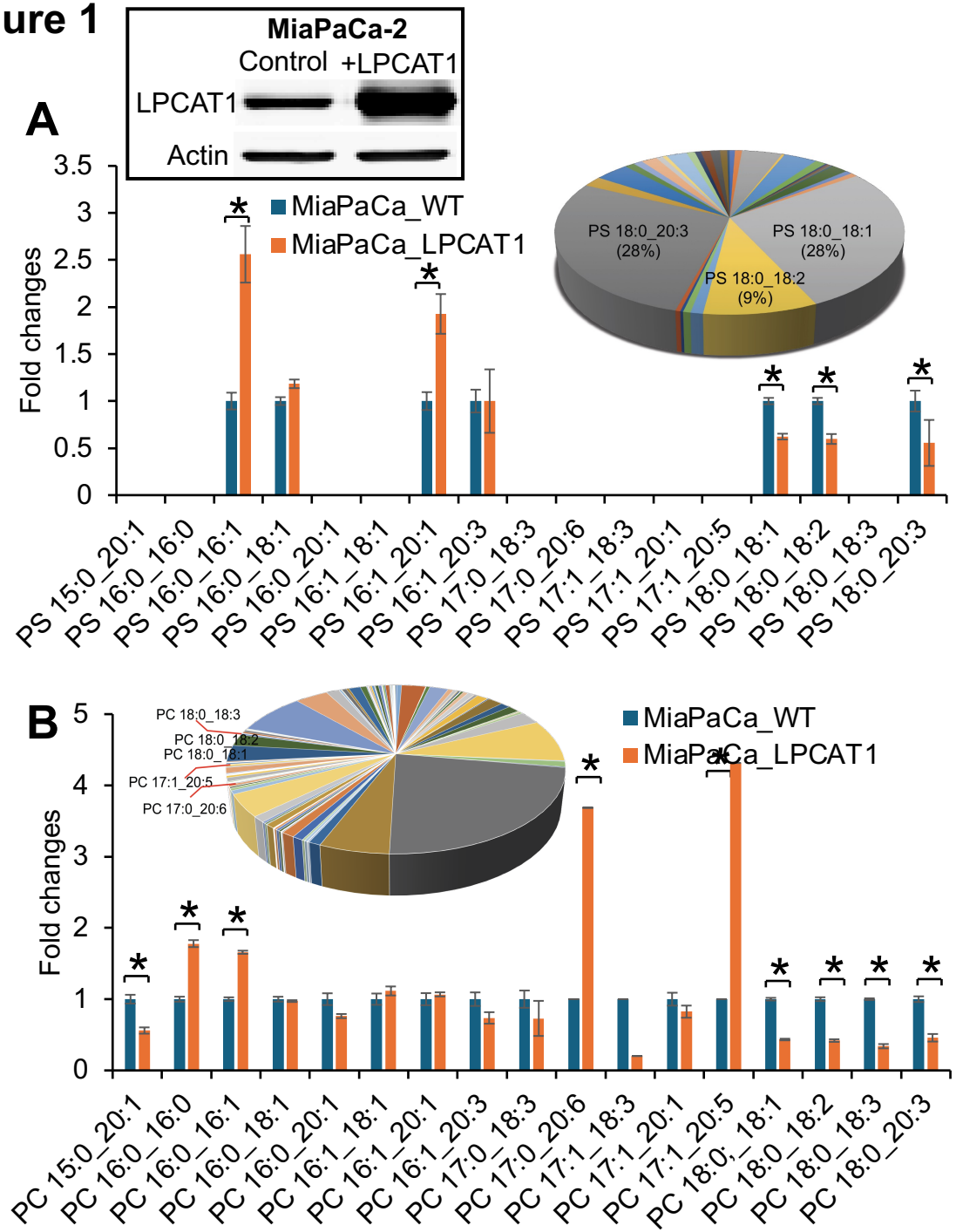
MiaPaCa-2
Control
+LPCAT1
LPCAT1
Actin
A
MiaPaCa_WT
MiaPaCa_LPCAT1
Fold changes
PS 18:0_20:3 (28%)
PS 18:0_18:1 (28%)
PS 18:0_18:2 (9%)
PS 15:0_20:1
PS 16:0_16:0
PS 16:0_16:1
PS 16:0_18:1
PS 16:0_20:1
PS 16:1_18:1
PS 16:1_20:1
PS 16:1_20:3
PS 17:0_18:3
PS 17:0_20:6
PS 17:1_18:3
PS 17:1_20:1
PS 17:1_20:5
PS 18:0_18:1
PS 18:0_18:2
PS 18:0_18:3
PS 18:0_20:3
B
PC 18:0_18:3
PC 18:0_18:2
PC 18:0_18:1
PC 17:1_20:5
PC 17:0_20:6
MiaPaCa_WT
MiaPaCa_LPCAT1
Fold changes
PC 15:0_20:1
PC 16:0_16:0
PC 16:0_16:1
PC 16:0_18:1
PC 16:0_20:1
PC 16:1_18:1
PC 16:1_20:1
PC 16:1_20:3
PC 17:0_18:3
PC 17:0_20:6
PC 17:1_18:3
PC 17:1_20:1
PC 17:1_20:5
PC 18:0_18:1
PC 18:0_18:2
PC 18:0_18:3
PC 18:0_20:3

Figure 2

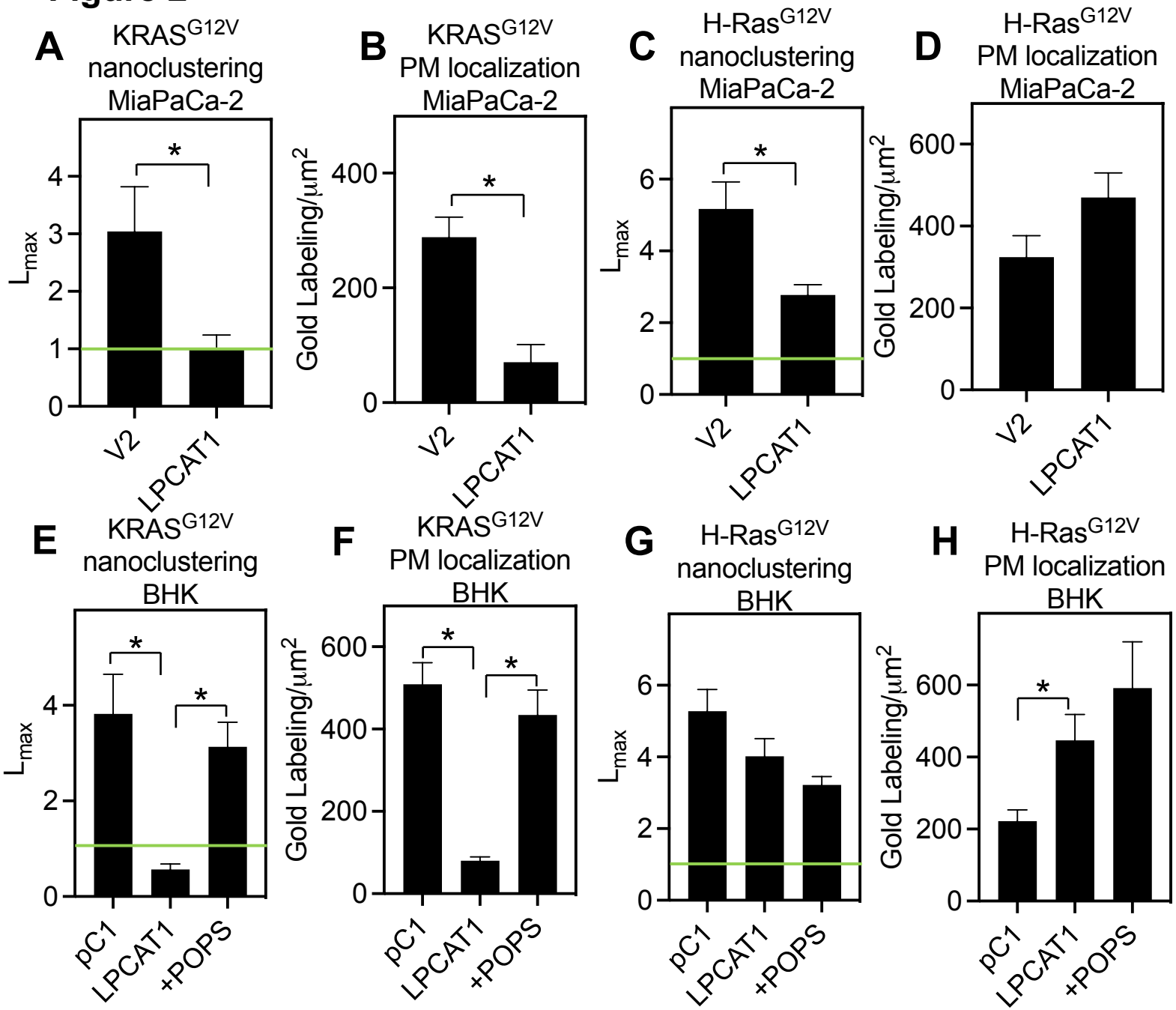
A
KRAS^{G12V} nanoclustering MiaPaCa-2
L_{max}
0
1
2
3
4
*
V2
LPCAT1
B
KRAS^{G12V} PM localization MiaPaCa-2
Gold Labeling/μm^2
0
200
400
*
V2
LPCAT1
C
H-Ras^{G12V} nanoclustering MiaPaCa-2
L_{max}
0
2
4
6
*
V2
LPCAT1
D
H-Ras^{G12V} PM localization MiaPaCa-2
Gold Labeling/μm^2
0
200
400
600
V2
LPCAT1
E
KRAS^{G12V} nanoclustering BHK
L_{max}
0
2
4
*
*
pC1
LPCAT1
+POPS
F
KRAS^{G12V} PM localization BHK
Gold Labeling/μm^2
0
200
400
600
*
*
pC1
LPCAT1
+POPS
G
H-Ras^{G12V} nanoclustering BHK
L_{max}
0
2
4
6
pC1
LPCAT1
+POPS
H
H-Ras^{G12V} PM localization BHK
Gold Labeling/μm^2
0
200
400
600
*
pC1
LPCAT1
+POPS

Figure 3

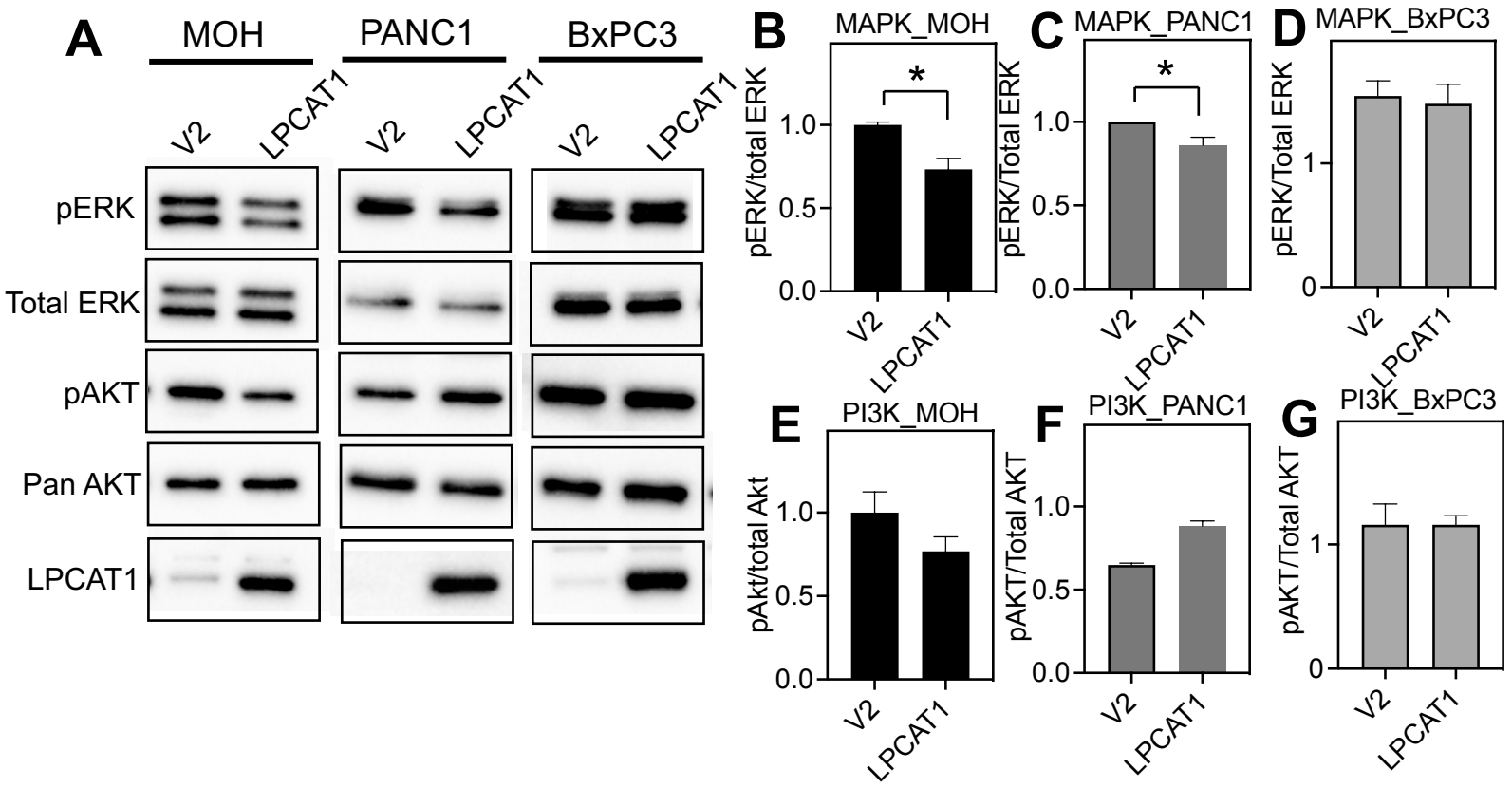
A
MOH
PANC1
BxPC3
V2
LPCAT1
pERK
Total ERK
pAKT
Pan AKT
LPCAT1
B
MAPK_MOH
pERK/total ERK
C
MAPK_PANC1
pERK/Total ERK
D
MAPK_BxPC3
pERK/Total ERK
E
PI3K_MOH
pAkt/total Akt
F
PI3K_PANC1
pAKT/Total AKT
G
PI3K_BxPC3
pAKT/Total AKT
*
*
0.0
0.5
1.0
0
1

Figure 4

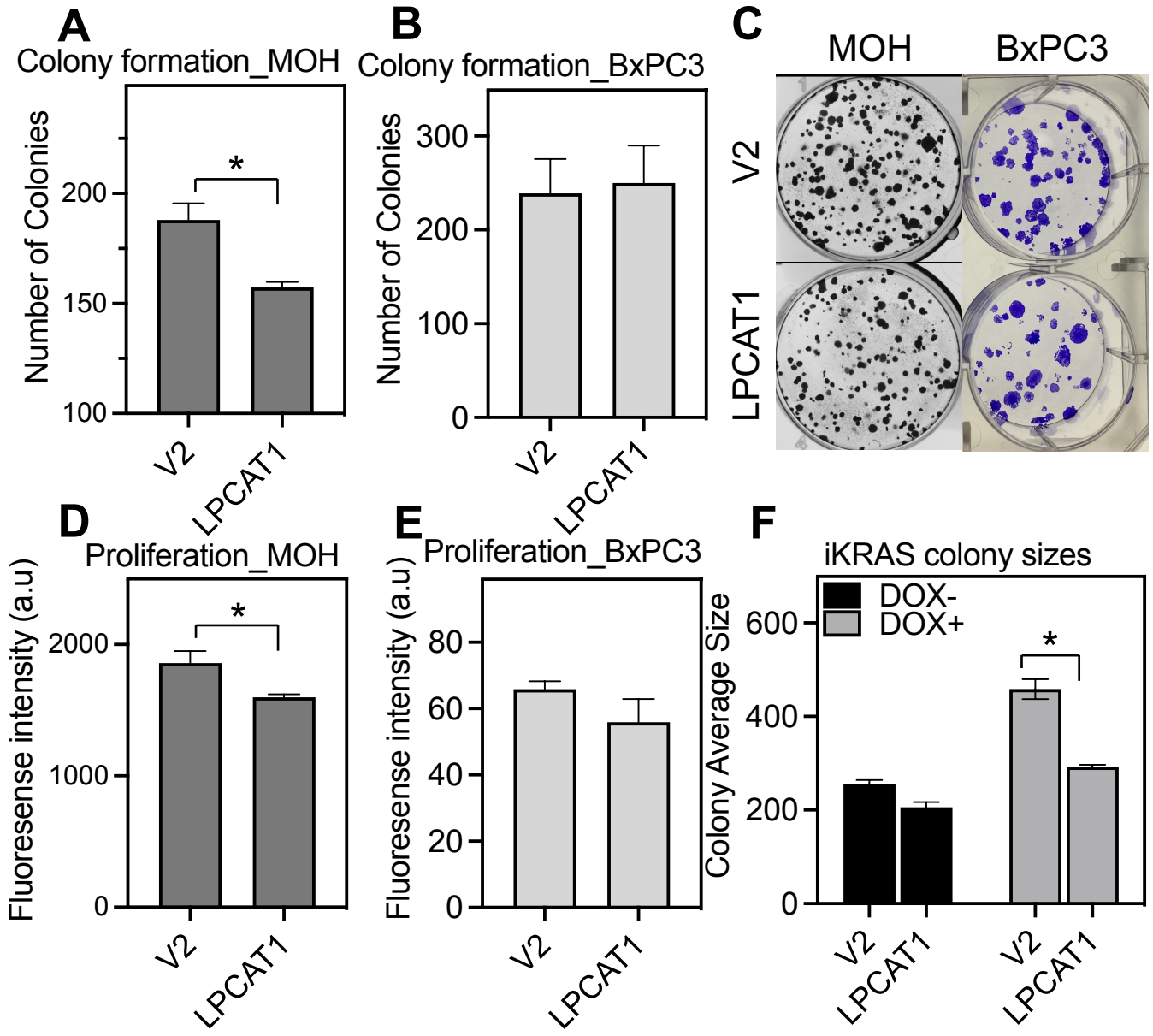
A
Colony formation_MOH
Number of Colonies
100
150
200
*
V2
LPCAT1
B
Colony formation_BxPC3
Number of Colonies
0
100
200
300
V2
LPCAT1
C
MOH
BxPC3
V2
LPCAT1
D
Proliferation_MOH
Fluoresense intensity (a.u)
0
1000
2000
*
V2
LPCAT1
E
Proliferation_BxPC3
Fluoresense intensity (a.u)
0
20
40
60
80
V2
LPCAT1
F
iKRAS colony sizes
DOX-
DOX+
Colony Average Size
0
200
400
600
*
V2
LPCAT1
V2
LPCAT1

Figure 5

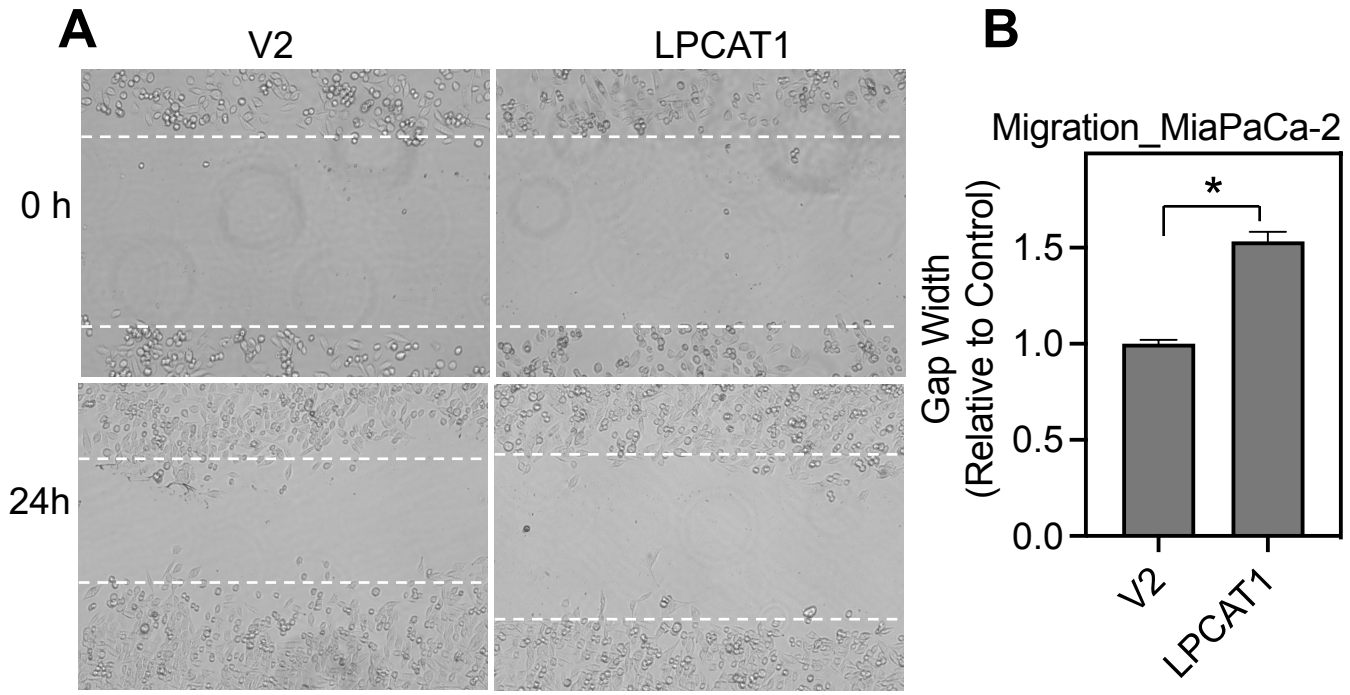
A
V2
LPCAT1
0 h
24h
B
Migration_MiaPaCa-2
Gap Width
(Relative to Control)
*
1.5
1.0
0.5
0.0
V2
LPCAT1

Figure 6

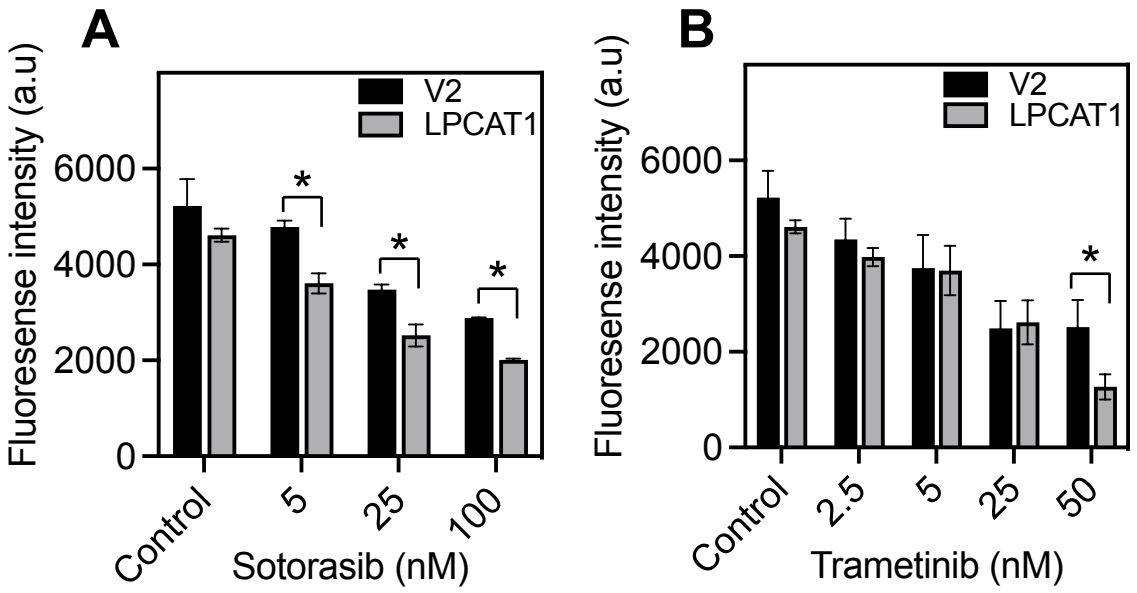
A
Fluoresense intensity (a.u)
6000
4000
2000
0
V2
LPCAT1
*
*
*
Control
5
25
100
Sotorasib (nM)
B
Fluoresense intensity (a.u)
6000
4000
2000
0
V2
LPCAT1
*
Control
2.5
5
25
50
Trametinib (nM)

Figure 7

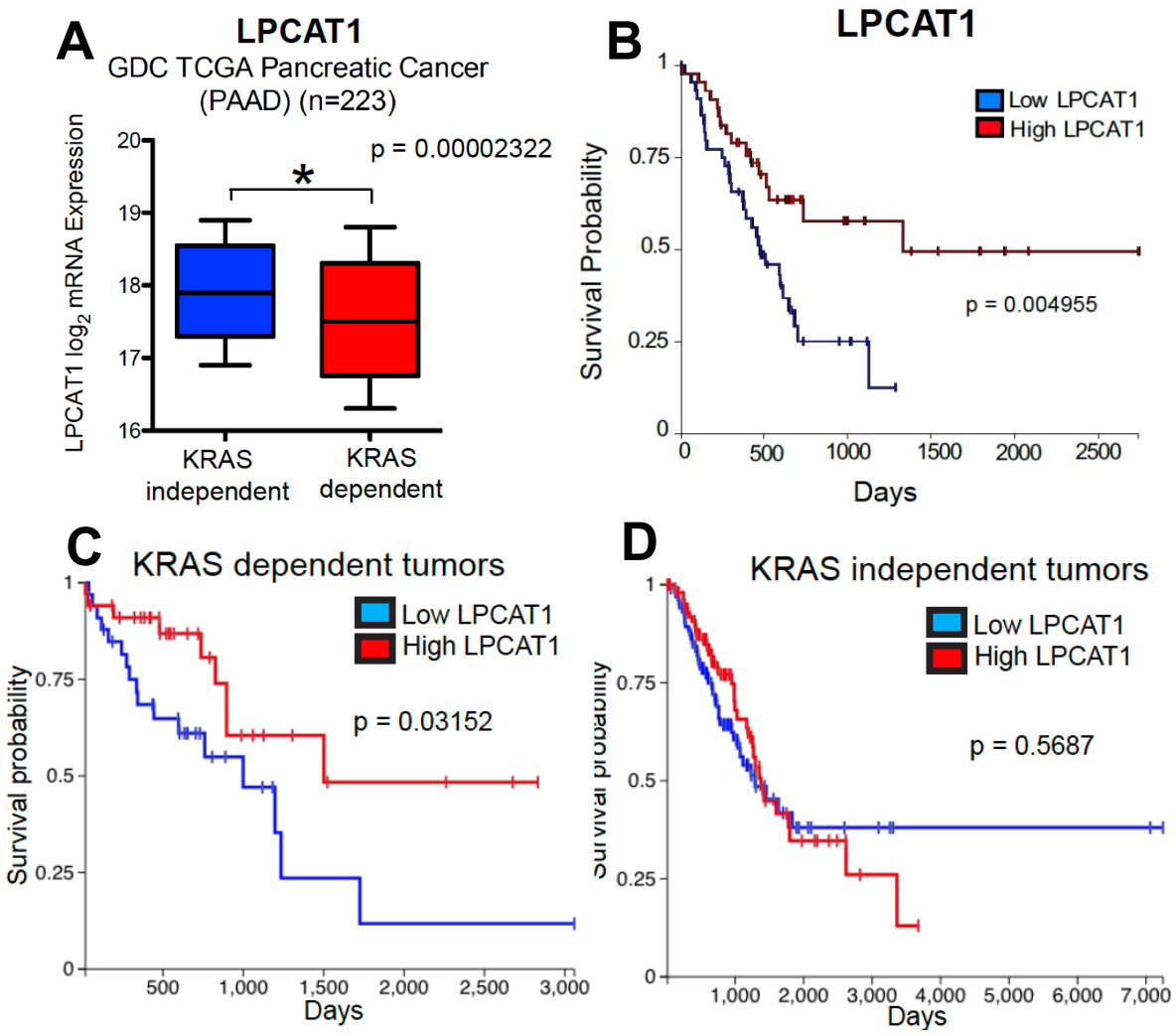
A
LPCAT1
GDC TCGA Pancreatic Cancer
(PAAD) (n=223)
LPCAT1 log2 mRNA Expression
p = 0.00002322
*
KRAS independent
KRAS dependent
B
LPCAT1
Low LPCAT1
High LPCAT1
Survival Probability
p = 0.004955
Days
C
KRAS dependent tumors
Low LPCAT1
High LPCAT1
Survival probability
p = 0.03152
Days
D
KRAS independent tumors
Low LPCAT1
High LPCAT1
Survival probability
p = 0.5687
Days